AD-A262 803

Coronal photometry and analysis of the eclipse corona of July 22, 1990

S. Koutchmy[1,5], R.C. Altrock[2,5], T. A. Darvann[3], N. I. Dzubenko[4], T. W. Henry[5], I. Kim[6], O. Koutchmy[7], P. Martinez[8], C. Nitschelm[1,9], G. A. Rubo[4] and J. Vial[10]

[1] Institut d'Astrophysique de Paris, CNRS, 98 Bis Bd Arago, F75014 Paris, France
[2] Phillips Laboratory (AFSC), Geophysics Directorate, Sunspot, NM 88349, USA
[3] University of Olso, Institute of Theoretical Astrophysics, P. O. Box 1029, Blindern N-0315, Olso 3 Norway
[4] Kiev University, Department of Physics, Kiev-252127, Ukraine. Russia
[5] National Solar Observatory/Sacramento Peak, National Optical Astronomy Observatories*, Sunspot, NM 88349. USA
[6] Sternberg Astronomical Institute, Moscow University, 119899 Moscow, Russia
[7] Univ. Pierre et Marie Curie, Laboratoire Analyse Numérique, Tour 55-65, 4 place Jussieu, 5éme étage, F-75230 Paris Cedex 05, France
[8] Ecole Nationale Supérieure de l'Aéronautique et de l'Espace, B.P. 4032, 31055, Toulouse Cedex, France
[9] Observatoire de Genève, 1290 Sauverny, Switzerland
[10] Institut d'Astrophysique Spatiale, Université Paris XII, Bat. 121. F-91405. Orsay Cedex, France

Abstract. — An extensive collaborative study of the maximum-type solar corona at the July 22, 1990 eclipse has been performed after collecting data from the ground and from an aircraft. The study provides photometric quality data and structural analysis on the electron corona. Synoptic data are used from the Emission-Line Coronal Photometer of the National Solar Observatory/Sacramento Peak. The activity of the low corona at the time of the eclipse is first discussed. Noticeable is a large nearby polar hole at the SSW limb well-observed on both synoptic green-line data and eclipse data. Strong activity is seen at the E and W limbs and numerous faint prominences are recorded all around the limb. The photometry of the White-Light corona has been performed with selected pictures from the French Falcon-20 aircraft experiment flown above Finland. Isophote maps are given as well as azimuthal scans in absolute units of average solar brightness. The standard flattening index is computed using the values determined for different radial distances. A few scans are compared with Fe XIV 530.3nm scans, and show great similarity when prominence emissions are excluded. The structural analysis is based on the excellent radially-filtered eclipse pictures obtained from the ground with one of the standard multi-station experiments placed along the path of totality in the USSR. Both the inner parts and especially the outer parts of the plasma corona are analyzed. Processed pictures to enhance small-scale gradients show the distribution of streamer-like structures and extremely fine rays. Despite a rather bright sky, long rays are seen up to $6R_\odot$; the origin of several very fine straight coronal threads is discussed as well as a system of voids seen above the East limb, surrounding prominence material

Key words: sun: corona - sun: total eclipse - sun: atmosphere - sun: activity - prominences - solar wind.

1. Introduction.

A total solar eclipse provides the unique opportunity of observing in white-light (WL) different parts of the solar atmosphere: the transition region, prominences, the hot electron K-corona, including the possible sources of the solar wind, and the dusty F-corona. The July 1990 eclipse did not occur in good conditions for ground based observations (Fiala et al. 1988). Therefore, an effort has been made to provide the best possible chance for a significant scientific return from observations made with portable equipment. namely to combine aircraft-based observation with ground-based observations made from multiple stations, with several instruments spread along the line of totality to increase the chance of having a clear sky. We note that no Spaceborne coronal experiment is available to provide information on the coronal activity in 1990.

Only snapshots of the corona are possible during an eclipse; the short duration of the event and the success of one experiment in our multi-station experiment permits

---

93   3   15   034

analysis at one single moment. More observations made around the eclipse data are needed to make the connection with disk activity; here an attempt is made to fully use the synoptic coronal data from the National Solar Observatory at Sacramento Peak (NSO/SP). The high resolution analysis of coronal WL structure of this near-maximum of sunspot activity will also be considered, as the eclipse provides a unique opportunity to image coronal structures from the solar limb to several solar radii, with good resolution. Special filter processing has been applied to enhance the density features seen in WL over the solar corona. We will confine the analysis to a few more quantitative parameters, leaving a more extended discussion of a maximum type corona until after the July 11, 1991 eclipse.

2. Observations of the corona at the 1990 eclipse and near the eclipse date

The material used in this work comes essentially from two different experiments performed at ground-based sites and with an airborne package.

2.1. THE FALCON JET ECLIPSE FLIGHT AND EXPERIMENT

We prepared a cluster of small telescopes put on an alt-azimuth mount behind 3 quartz optical windows of different diameters (220 mm; 120 mm and 80 mm). The main telescope was a 160 mm-aperture Cassegrain telescope put behind the largest window. The pointing was done manually, thanks to a small guiding telescope feeding a color video-CCD camera. The trajectory of the eclipse flight had been accurately computed, taking into account the local conditions of flight, in order to guarantee a stable image during the 80 sec of totality. It was dediced to perform the flight above Finland because the line of sight (l.o.s.) was sufficiently low to allow a l.o.s. almost to the side-on windows. However, even at the high altitudes made possible with a jet like the Falcon 20, atmospheric attenuation is still a problem with regard to photometric accuracy, in the case of low elevation objects. For this reason, the atmospheric spectral transmittance of the Earth atmosphere for the expected elevation (3°) was computed for different altitudes, see Figure 1a, using a standard model of the atmosphere and the LOWTRAN 6 package provided by Geophysics Laboratory (AFSC). The computation clearly shows the effect of ozone absorption at high altitudes. Figure 1b shows the spectral transmittance recomputed for the local conditions of the eclipse flight which occurred at 12 km above Joensuu (Finland). The recorded time of second contact was 01:52:45 U.T., and the length of totality was only 73 sec instead of 80 sec we were expecting. The altitude of the Sun was 4° and azimuth angle 52°. Many experiments we had prepared

failed to give scientifically useful data because a few minutes before totality our optical windows became frozen from the inside, so it was dediced to concentrate on a freeze-free window and run only the WL photographic experiment to provide absolute and relative calibration for coronal pictures of very limited resolution. Pictures were taken with color films of high sensitivity with different exposure times, and calibration was made with a specially designed sensitometer. Selected pictures were analyzed with the fast microphotometer at National Solar Observatory/Sacramento Peak. A sample of the pictures we took can be found on the cover of the Sept-Oct 1990 issue of the French journal: l'Astronomie 104 or in Sky and Telescope Jan. 1991, 81 87-88.

2.2. THE GROUND-BASED RADIAL FILTER CORONAL IMAGING

A multi-station experiment was attempted, based on an experiment run at past eclipses (Koutchmy et al. 1974). Eclipse teams from France, Czechoslovakia, and the ex-USSR were based at 3 different widely separated locations in USSR, but only the team of Kiev University, led by N.I.D. and G.A.R., succeeded in getting some good data although on a rather bright sky. One of the original radially-compensated pictures obtained on Ekta 64 color film sheet with a 20sec exposure time was transmitted for analysis. A color reproduction of the picture can be found on p. 105 of Sky and Telescope (1991) 81. The picture is not well-suited for photometric purposes but it is sufficient for the morphological analysis. Black and white duplicates with different color filters were made on the 18 × 24 cm film sheet, and the best-spatial-resolution duplicate, made with a broad-band green-orange filter, was scanned with the fast microphotometer of NSO/SP. The resulting intensities correspond well to the WL corona as the main low-excitation emission lines are excluded.

The picture was taken at 03:05 U.T. From a site situated near the village of Markovo (N 64°40.0, E 170°24.0), the altitude of the Sun was 40°. The radial filter transmission has already been described by Kouchtmy et al. (1978). A Zeiss achromatic AS doublet lens of 20 cm aperture and 3 m focal length was used to produce the coronal image.

2.3. SYNOPTIC OBSERVATIONS OF THE FEXIV CORONA AT THE TIME OF THE ECLIPSE

Observations were made at NSO/SP with the Fisher-Smartt Emission Line Coronal Photometer (ELCP) (Smartt, 1982). This instrument photoelectrically records the solar corona when fed with the John W. Evans Solar Facility 40 cm Coronagraph. It operates at high precision due to its ability to subtract the sky background from the signal in emission lines through use of a lock amplifier

oscillating at a rate of 100 kHz between the continuum and the line at 530.3 nm (Fe XIV), which is formed at an approximate temperature of 2 MK. Observations in other lines will not be discussed in this paper. Successive scans are reproducible frequently to less than 1 millionth of the brightness of the solar disk at the given wavelength. Scans are routinely made in skies as bright as 200-400 millionths. A 1.1 $(0.07R_\odot)$ arcmin aperture is scanned around the limb at 1.15, 1.25 and $1.35R_\odot$. The output of the ELCP is sensed by a photomultiplier, digitized and recorded every 3° of latitude. Absolute intensities in millionths of the brightness of the center of the disk 530.3 nm are obtained by calibrating the system through a neutral density filter.

3. Results

3.1. ISOPHOTE MAPS AND THE FLATTENING INDEX

We selected the best airborne WL pictures taken with 300 mm focal length lens on 35 mm and 70 mm films to perform a photometric analysis. Pictures were scanned with the equivalent of a blue-green filter, in order to reduce the effect of over-exposed images of red prominences, which are seen all around the lunar limb. Figure 2 gives the isophote map obtained from a short exposure picture and Figure 3 the isophote map obtained from a picture with longer exposure time made on film pushed at 3200 ASA. We do not show the corona further out, because the influence of corrections to be made for scattered light in the combination window-lens are large and reduce the precision. The influence of the sky background is negligible here, and no asymmetry of non-coronal origin is detected over the isophote map. In figure 4 we give few typical scans calibrated in intensities along different directions to illustrate the polar-equatorial asymmetry measured in this solar-maximum corona.

To go further in the analysis of the polar-equatorial asymmetry, a statiscally more significant parameter, the well-known flattening index ϵ (Koutchmy & Nitschelm 1984), is derived in Figures 4 and 5. This index is widely used to describe the solar-cycle related variations of the K-corona. The radial variation, assuming a linear relationship for ϵ, has been extrapolated to the radial distance $R = r/R_\odot = 2$ to deduce the so-called $(a + b)$ value in Figure 5. Only the very inner part of the corona, between $R = 1.2$ and 1.4, has been used to deduce $(a + b)$, which makes the result rather uncertain. Note that points corresponding to $R > 1.4$ are affected by the brightness of the F-corona and we wanted to deduce the flattening at $R = 2$, or equivalently $(a + b)$, for the electron K-corona.

3.2. RELATIVE AND ABSOLUTE PHOTOMETRY

A classical way to present the distribution of WL intensities in the corona is to show the azimuthal variations of intensities for selected radial distances. This is espe-

cially convenient in the inner parts of the corona where the radial variations are rather drastic. Figure 6 presents the azimuthal variation of relative intensities at several values of R as measured on a filtered picture in blue-green color. The coronal hole (CH) at 190° position angle (near the S-pole) is easily seen on these scans, up to $R = 1.5$. Further out, the dusty F-corona dominates, so the CH becomes dimmer. After substracting the parasitic scattered light, as observed on the lunar background, and using a calibration curve built by introducing the so-called Baker densities, we converted the measured intensities over the pictures to absolute units of the average brightness of the solar disk observed with same blue-green color filter (broad band WL photometry). The selected scans are shown on a low-contrast print of the coronal picture in Figure 7. To display the whole range of intensities observed from the inner parts to the outer-most parts at $R = 3.0$, we show in Figure 8 a logarithmic display of the azimuthal variations of intensities, the unit being 10^{-8} of the average solar brightness B.

In both Figures 6 and 8, the position angles have been determined by identifying the prominences observed in the very inner parts of the corona, the position of filaments reported from ground-based non-eclipse observations made at different observatories are taken into account. The precision of positioning is estimated to be $\pm 2°$. Concerning absolute intensities, taken into account all sources of uncertainties, we estimate that errors in Figure 8 amount to $\pm 30\%$ for the inner parts of the corona, coming down to $\pm 15\%$ for the outer, although noisier, parts of the corona. The relative variations of intensities are certainly more precise, reaching a $\pm 5\%$ precision for local inner features. To reach a better precision, a longer focal length picture is needed and a more precise method of absolute calibration using field stars (Koutchmy et al 1978, and Lebecq et al 1985), should be used. This is difficult to perform with an airborne experiment. Additionally, the non-optimum conditions of observations for this eclipse flight, when the main window we used left only a small portion unfrozen, did not permit a high photometric accuracy and did not permit the analysis of the outer-most parts of the corona. However, we note that through the standard non-optical windows of the aircraft, coronal streamers could be visually seen at large radial distances. Thus if in the future the problem of keeping the optical windows clean can be solved (using a forced flow of dry CO_2 gas, for example), a far more precise photometry of the external parts of the corona can be done.

3.3. SYNOPTIC MAPS AND THE LARGE FEATURES OF THE JULY 22, 1990 CORONA

The Fe XIV green-line emission picture and map, produced to give the best representation of the coronal emission at the time of the eclipse, are presented in Fig-

ures 9 and 10. Figure 9, which shows the intensity from $R = 1.15$ to 1.35, compares favorably with the eclipse data of Figure 2 and even Figure 7. The SSW polar CH is particularly well observed by both eclipse and out-of-eclipse observations. Its position can be easily identified on the synoptic map represented in Figure 10. This is a major feature of the July 1990 corona, which occurred close to the sunspot maximum of activity. Another major feature present on Figure 10 is the E-limb strong enhancement of Fe XIV emission occuring near P.A. 115° being more prominent than the W limb features. Comparing Figure 11 (Fe XIV emissions) and Figure 6 (WL intensities) for the same radial distances, we tried to look more carefully at the distribution of WL intensities for small values of R. Figure 12 presents the result of the analysis at small R: 1.05; 1.10 and 1.15. The large effects produced by the prominence emissions is apparent on scans performed at $R = 1.05$ and even $R = 1.10$. They suggest that at least a part of the strong inner-corona Fe XIV emission seen on the E-limb and the inner Fe XIV emission seen at the west limb at 30° S could well come from active regions enhancements with a prominence inside. The large dynamic range of the Fe XIV observations relative to the WL observations is due to the fact that Fe XIV emission is proportional to $(n_e)^2$, and WL to n_e. A recent re-analysis of calibration procedures indicates that all intensities in Figures 9, 10 and 11 should be multiplied by 0.67.

3.4. FINE SCALE STRUCTURES USING THE HIGH RESOLUTION GROUND-BASED PICTURE

We used the radially filtered picture to analyse the fine scale details of the eclipse corona. Figure 13 is a print made from the best duplicate, after digitization and data processing using simple operators to remove artifacts and to enhance the small scale gradients in all directions. Unfortunately, such procedure increases also the influence of the photographic noise. A white disk has been also generated to show the location and the size of the solar disk, in superposition on the Moon's disk. Note the dominant radial structure and the location of the CH at the SSW. Besides a few large scale structures, which could be a "system of streams" forming together what is called in the literature a coronal streamer (for example, at the SW limb), several regions show many straight "streams" or "rays", which are rather small in cross section but extended in the radial direction. The most remarkable ensemble of such tiny extended rays is seen in the SWW region. Figure 14, which is a variant of Figure 13, shows these structures even better. A special image-processing operator (Koutchmy & Koutchmy 1990) has been applied to the image represented by a 1024 × 1024 pixel matrix of intensity value, namely the operator *Max* applied to the absolute values of second derivatives computed in 8 different directions for each pixel. At the SW on Figure 14, an

elongated ray out to $R = 6$ with a tiny cross-section is revealed. Note that the ray seems to emerge from a coronal region with small loops (in the inner parts of the corona, the noise is considerably reduced compared to what is present in the external part, so almost all features seen on Figure 14, especially the very inner parts, are real coronal details). Even more remarkable is the ensemble of curved tiny rays streching out from the W limb. Many more rays are seen all around and sometimes a detached struture can be noticed, for example above the N-pole region.

4. Discussion

The main results of the analysis of the large-scale features of the inner corona concern: the measurement of the flattening index of the near-maximum-activity corona; the occurrence of the rather large coronal hole, an observation confirmed by the out-of-eclipse synoptic analysis of the Fe XIV emissions; the importance of the line emissions recorded on the broad-band WL pictures, due to the presence of numerous large or faint prominences all around the limb.

4.1. GLOBAL PARAMETERS

The rather limited precision of our absolute calibration does not allow us to reliably compute the magnitude of the WL flux of the eclipse corona, however, several regions at low latitude clearly show large intensities, revealing a large amount of material above active regions (enhancements). The flattening index determination is based only on relative intensity measurements (indeed, the use of isophote maps), so there a satisfactory precision is attained, providing monochromatic emissions from faint prominences are avoided. The value of ϵ we deduced at $R = 2$, the so-called $(a + b)$ value, is typically 0.12. This value is an agreement with values reported in the literature for an active corona (Loucif & Koutchmy 1989) but lower than the typical values obtained for a minimum corona with polar coronal holes. However, an extrapolation made in this last work (see their Fig. 7b) at the time of a pre-maximum corona, would give a lower value, close to 0.07 on average, although a large dispersion is present. Because the current sunspot cycle is not yet over, it is difficult to speculate on the origin of the discrepancy: is it because we did not yet reach the true maximum of activity in July 1990, or is it because our value of ϵ is too high due to errors produced by the procedure we used? Note on Figure 5 that the extrapolation to $R = 2$ is based on points situated between $R = 1.2$ and 1.4 only; including a few points up to $R = 1.5$ would drastically lower the $(a + b)$ value! This makes the determination of $(a + b)$ very sensitive to the details of the inner corona, a part of the corona that is presumably free from the influence of the F-corona, which is circularly symmetric (at these radial distances).

Finally, we note that the presence of the large S-pole CH is an important factor determining the value of $(a + b)$; obviously, without the CH, the corona would have shown a more "normal" (namely lower) flattening index.

4.2. PHOTOMETRIC ANALYSIS

Commenting further on the inner-corona WL intensity distribution, we note definitely higher values at the W limb than the E limb, when emissions from faint prominences are avoided (cf. Figs. 6 and 12). This is clearly different from what was observed in the Fe XIV 530.3 nm line emissions taken a few hours before the eclipse (cf. Figs. 10 and 11); there the E limb is definitely brighter, especially at position angles near 115° (EES limb). A qualitative agreement is, however, readily noticeable, even at $R = 1.15$, when the overall distribution is considered. The correlation between WL intensities and Fe XIV line intensities is clearly lower in the very inner corona, where temperature inhomogeneities are present, especially over active regions, than in the higher corona. At radial distance $R = 1.35$, the correlation appears better: the W limb is now brighter on both WL and Fe XIV intensity distribution, and the qualitative agreement is very good (cf. Figs. 6 and 11). It is quite interesting that the lower correlation found in the very inner corona coincides with the presence of many faint prominences, including those which are entirely connected with active regions, revealing the large temperature inhomogeneities above the regions. A closer examination of the best radially-filtered picture confirms this statement, showing even more details on the influence of faint prominences. Figure 15 shows an enlarged part of the inner corona at the EEN limb where significant WL enhancements are observed from $R = 1.15$ to 1.5 (cf. Fig. 6). Fe XIV line emissions do not show prominent enhancement (cf. Fig. 11). However, two large but rather faint quiescent prominences are recorded there. We also identify several regions above these prominences which are definitely dark on Figure 15, revealing a large deficit of electron density. These regions look like parts of a dome with voids covering each prominence, as described by Noëns (1990). With a cruder spatial resolution we would have said they are the cavities sometimes observed under the helmet streamers; here we observe also narrower streamers and complex empty regions. Note in Figure 13 that a more classical helmet streamer, composed of the superposition of several extended streams over a small faint prominence with a possible cavity, is observed at the SE limb. Examining the detailed magnetic field maps from NSO/Kitt Peak, as well as the reconstructed synoptic maps as published, for example, in Solar Geophysical Data (NOAA), for the period of July 1990 eclipse, we found it rather difficult to form any definite conclusions concerning the association of neutral lines and concentration of opposite-polarity magnetic fields with coronal features.

This conclusion was recently reached by other observers, who analyzed a simpler corona closer to the sunspot minimum of activity (Sime et al. 1988). In the last year, it has become more and more evident that even the K-corona is very inhomogeneous and variable. Above active regions, large-amplitude kG coronal magnetic fields are observed in both the radio spectrum (White et al. 1991) and the optical spectrum (Koutchmy & Zirker 1990). At the sunspot maximum of activity, a large number of transient events, connected with prominence eruptions near active regions, are observed (MacQueen & Fisher 1983). On a snapshot, as observed during an eclipse, it is impossible to consider those events, but their influence is certainly imprinted on the coronal image. So it seems rather futile to go further with an exercice that consists of connecting each coronal feature with "something" on the disk as guessed from observations made several days before or after the eclipse.

4.3. STRUCTURAL ANALYSIS

A last but fundamental point should now be considered, namely the fine structure illustrated by Figures 13 and especially 14. Many thread-like or ray-like features are observed; should they be considered as sheets extending beyond the resolution limit (10Mm) seen side-on or are they of circular cross-sections? Are they crossing each other? Additionally, we have examples of a ray extending at least to $R = 6$ (neglecting projection effects which can make the ray only more extended). The long ray at the SW limb in Figures 13 and 14, slightly curved in the inner corona, straight above and with a seemingly decreasing cross-section, is probably the best example on this eclipse picture. Above this ray, many other rays emanating from the W limb are detectable, some of them appearing almost parallel but again slightly curved in the inner part of the corona and never strictly radial. Many other examples, even above the N-polar region, can be found; sometimes these rays seem to be detached and they appear to begin at a significant radial distance (see above the E limb). We do not believe those rays have a circular cross-section; in many cases only one edge of the ray is sharp which could reveal a tangential discontinuity. We have a strong suspicion that each sharp edge corresponds to a jump of the magnetic field amplitude; conservely, a fine ray could correspond to the location of a neutral sheet and reconnection phenomena could occur along it in the quasi-radial direction, the neutral sheet being stretched out by the wind and gravity. An even more radical hypothesis can be considered: the existence of the so-called High Coronal Flare (Cliver & Kahler 1991). Our picture (Fig. 14) of a corona filled with many such rays supports this hypothesis.

5. Conclusion

Calibrated eclipse pictures permit an analysis of the large-scale features; this analysis is especially interesting when additional information on the corona is available from observations made around the time of the eclipse. However, only high-resolution radially-filtered pictures permit access to the real physical processes responsible for the coronal structure. A temporal coverage at scales of order of few hours is needed to make a further progress: this is the aim of the multi-station international experiment ran at the July 11, 1991 total solar eclipse. Furthermore, large aperture telescopes like the Canadian-French-Hawaiian Telescope have been used during that eclipse, so we plan to perform measurements with a significantly better spatial resolution which, hopefully, will be sufficient to resolve a few of the density structures linked with magnetic reconnection phenomena. The very existence of the fine structure of the corona seems, however, to represent a rather formidable challenge for theoretical consideration. Apart from eclipses, progress in coronal physics will continue to depend, as far as magnetic field measurements are concerned, on the development of a large aperture mirror - corona-graph and for other diagnostics, on sophisticated spaceborne experiments planned on the SOHO spacecraft.

References

Billings D.E. 1966 A Guide to the Solar Corona NY Acad Press

Cliver E. and Kahler S. 1991, ApJ 366, L 91

Fiala A.D., Bangert J.A. and Harris W.T. 1988, US Naval Obs., Circular No. 173

Koutchmy O. and Koutchmy S. 1989, in 10th SPO Workshop Proceedings, O. von der Lühe, (Ed. NSO) 217

Koutchmy S., Dzubenko N.I., Nesmjanovich A.T. and Vsekhsvjatsky S.K. 1974, Solar Phys. 35, 369

Koutchmy S., Lamy P., Stellmacher G., Kouchtmy O., Dzubenko N.I., Ivanchuk V.I., Popov O.S., Rubo G.A. and Vsekhsvjatsky S.K. 1978, A&A 69, 35

Koutchmy S. and Nitschelm C. 1984, A&A 138, 161

Koutchmy S. and Zirker J.B. 1990, Lect. Notes Phys 363, 242

Lebecq C., Koutchmy S. and Stellmacher G. 1985, A&A 152, 157

Loucif M.L. and Koutchmy S. 1989, A&AS 77, 45

MacQueen R.M. and Fisher R.R. 1983, Sol. Phys. 89, 89

Noens J.C. 1990, private communication

Sime D.G., Fisher R.R. and Mickey D.L. 1988, ApJ 33, L-103

Smartt R.N. 1982, Proc. SPIE 331, 442

White S.M., Kundu M.R. and Goplaswamy N. 1991, ApJ 366, L-43

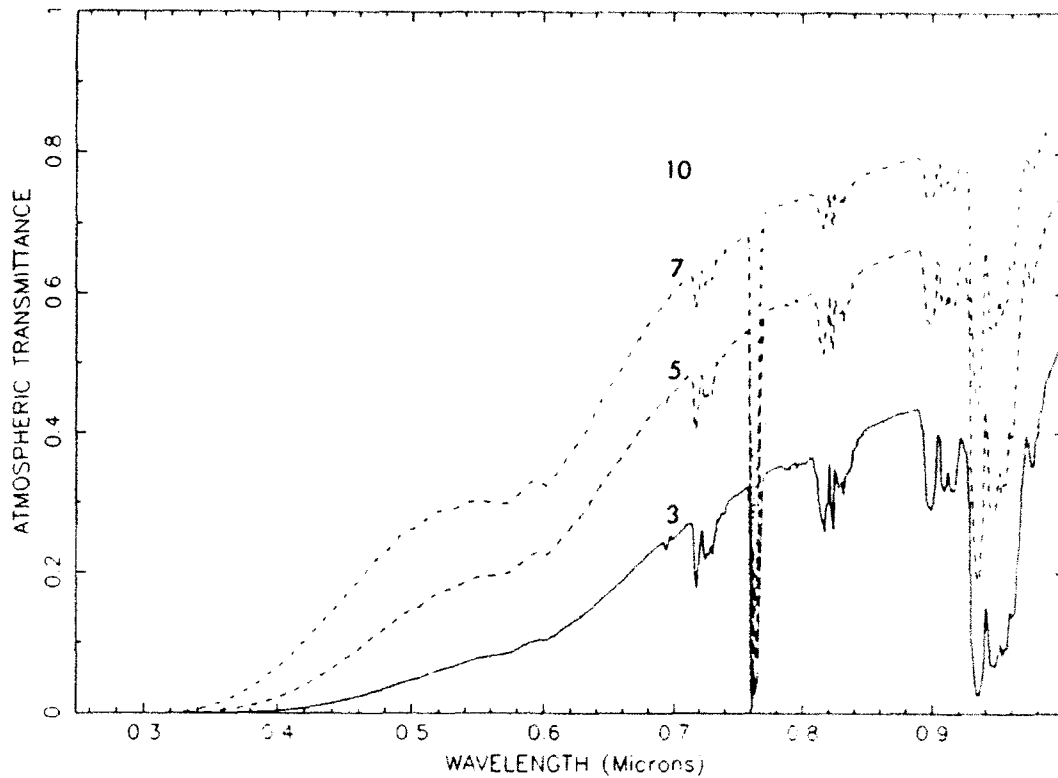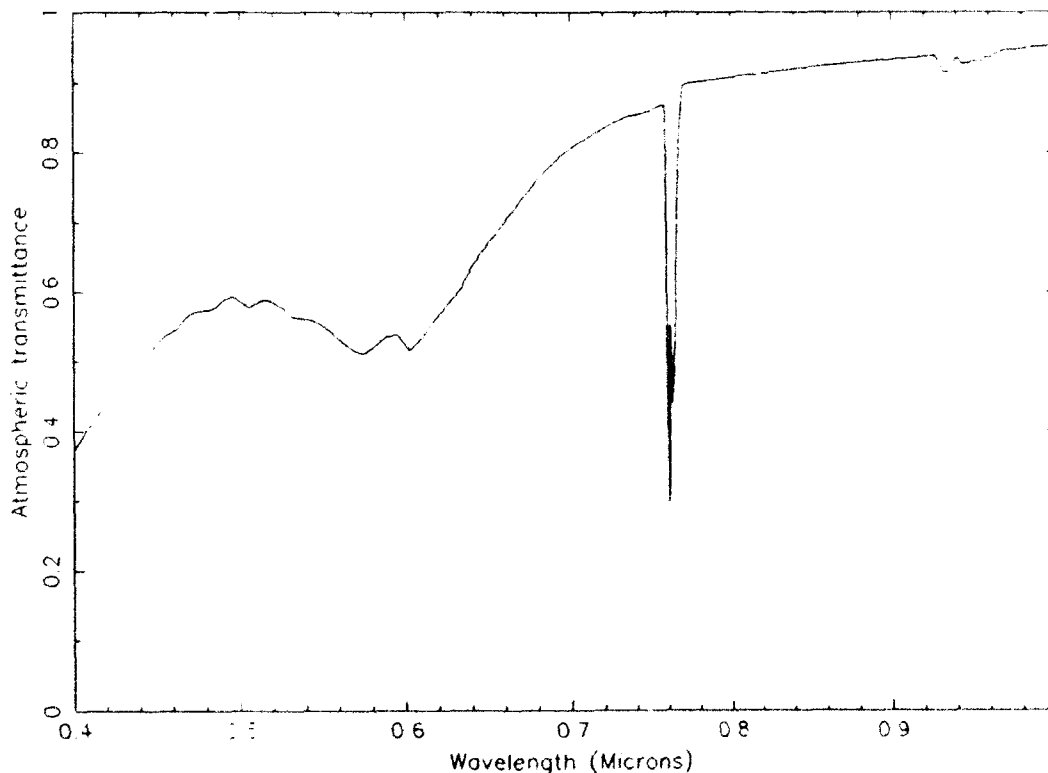TRANSMITTANCE (3° height, rural, Summer)

FIGURE 1a. Spectral transmission of the Earth atmosphere computed for different altitudes above sea level. Altitudes on the curve are given in km and the line-of-sight is assumed to have a height of 3° above the local horizontal direction. The dip at 0.76 microns is due to the molecular absorption of O_2.

TRANSMITTANCE AT 12 KM ABOVE JOENSUU (Summer, Rural, h=4°)

FIGURE 1b. Spectral transmission computed for the actual eclipse flight. Note the absorption near 600 nm produced by the ozone layer.

CONTOUR PLOT, CORONA JULY 22, 1990

FIGURE 2. Isophote map produced after recording coronal intensities from the inner corona (short-exposure) picture obtained with the airbone experiment; the effective spectral range covers the blue-green region. N is at the top, and E at left.
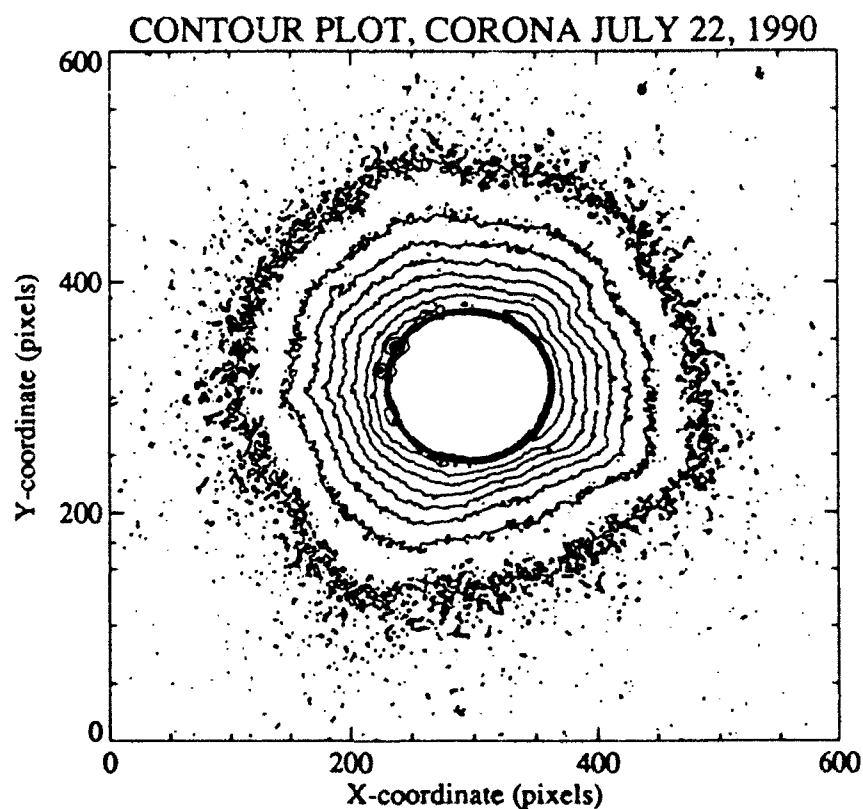
CONTOUR PLOT, CORONA JULY 22, 1990

FIGURE 3. As Figure 2, for the outer corona (long exposure). Note the different scale.

FIGURE 4. Typical and average radial scans performed near the equatorial and polar directions on the picture used for Figure 2 and the deduced flattening index.
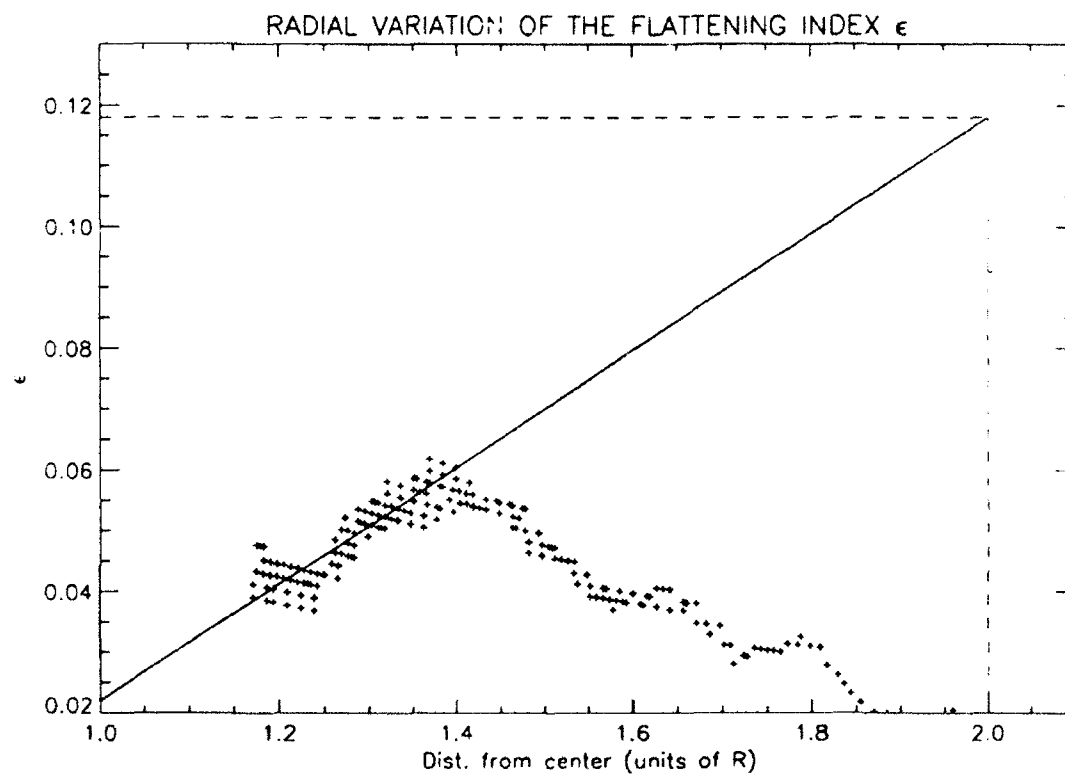
FIGURE 5. Extrapolation of the radial variation of the flattening index to show the possible value for the K-corona alone at $R = 2$.
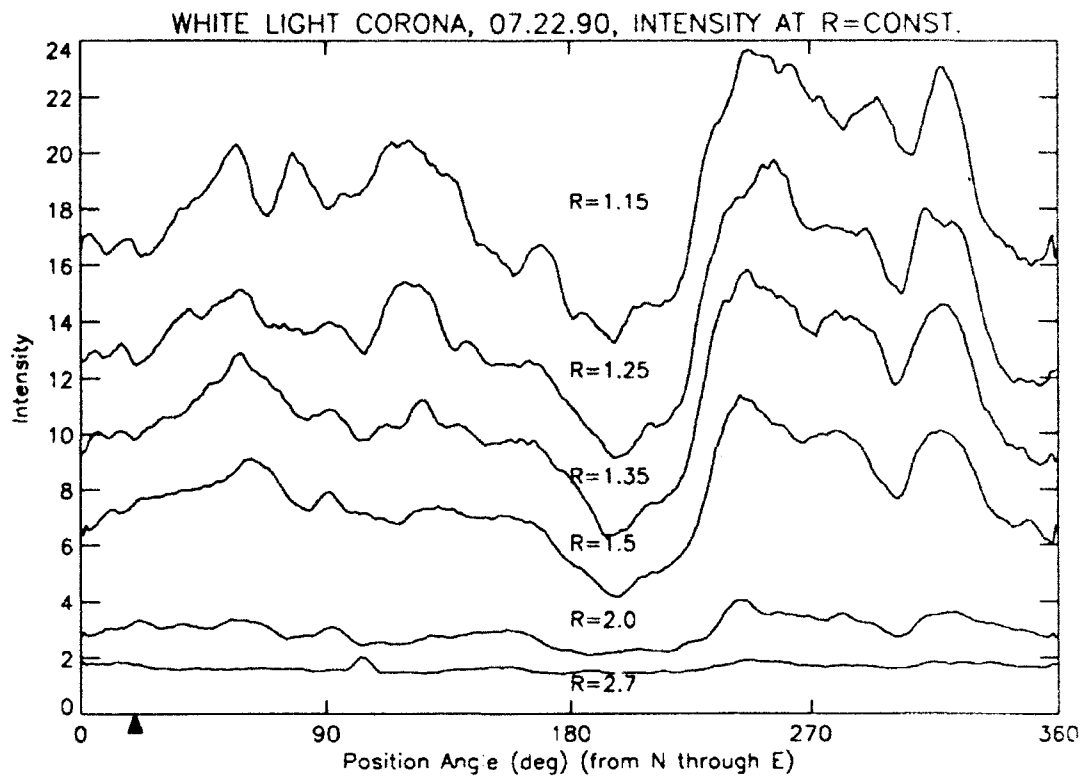
WHITE LIGHT CORONA, 07.22.90, INTENSITY AT R=CONST.

FIGURE 6. Azimuthal variation of the measured intensity in the inner corona for different radial distances (airborne experiment). Intensities are linear but in relative units; the exact position of the heliocentric N is shown by a small mark under the abscissa near the 20° position angle.
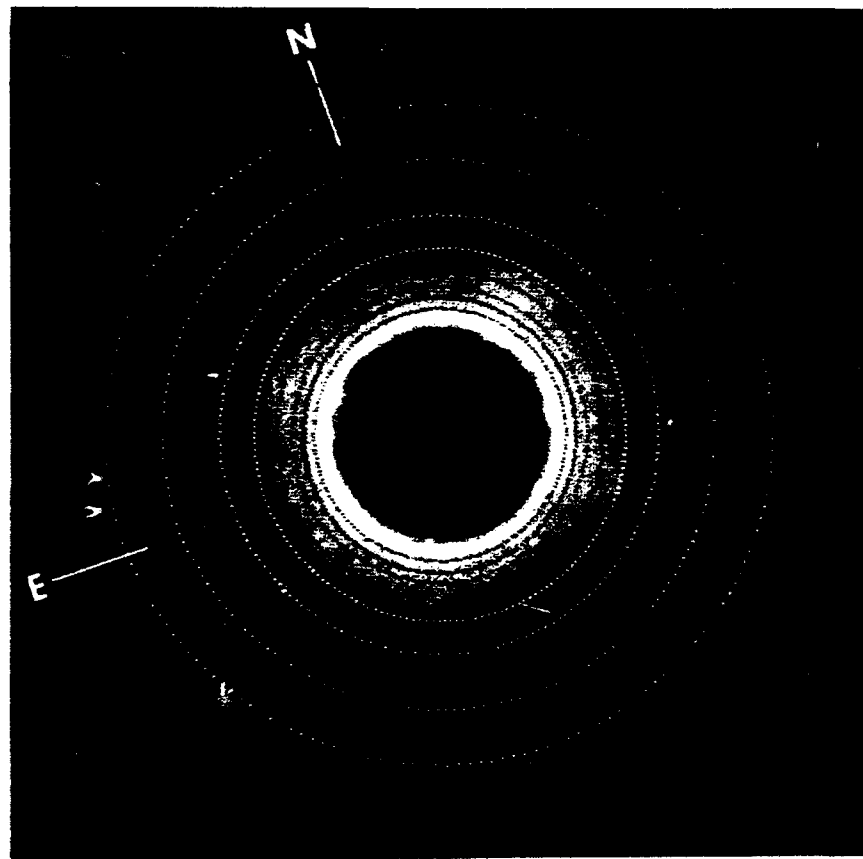

FIGURE 7. Picture reproduced from the recorded intensities of the coronal picture used for Figure 3 with azimuthal selected scan heights shown with dotted lines; radial distances correspond to the scans shown in Figure 8. Note the exact position of the N pole and E limb.

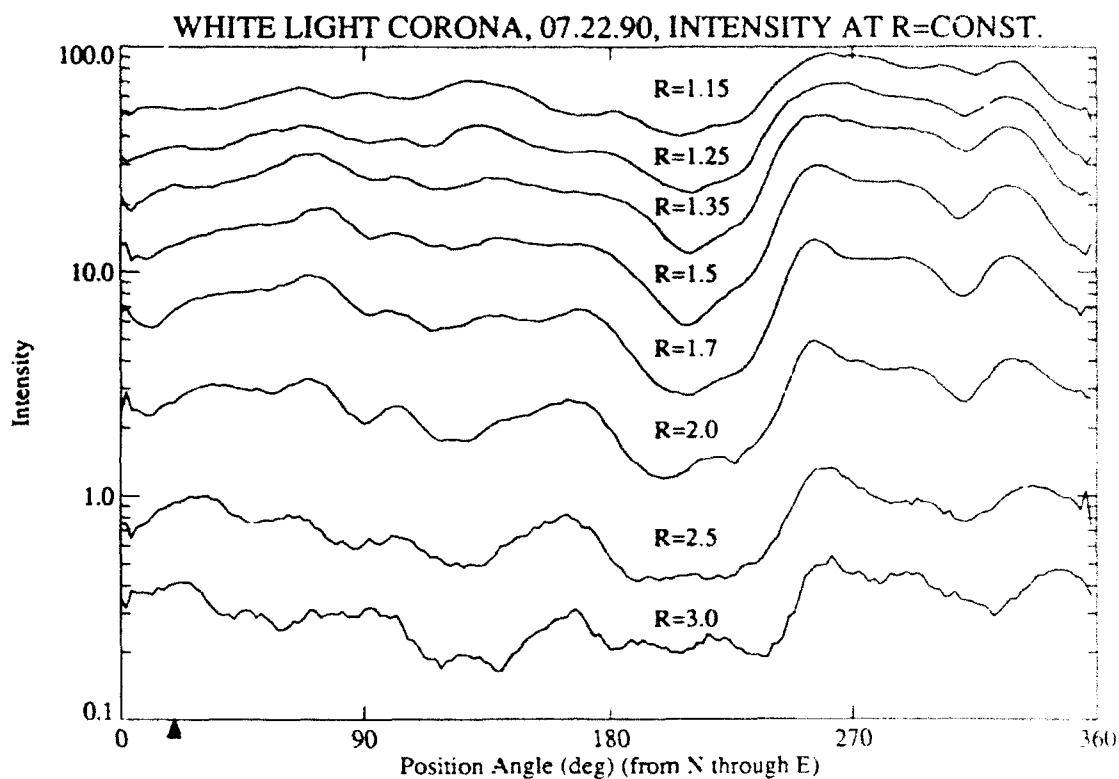## WHITE LIGHT CORONA, 07.22.90, INTENSITY AT R=CONST.

FIGURE 8. Azimuthal variation of coronal intensities for different radial distances on a *logarithmic* scale. Intensities are given in absolute units of 10^{-8} times the average brightness of the solar disk; instrumental scattered light was removed. Exact positions of N is near the $20°$ mark.
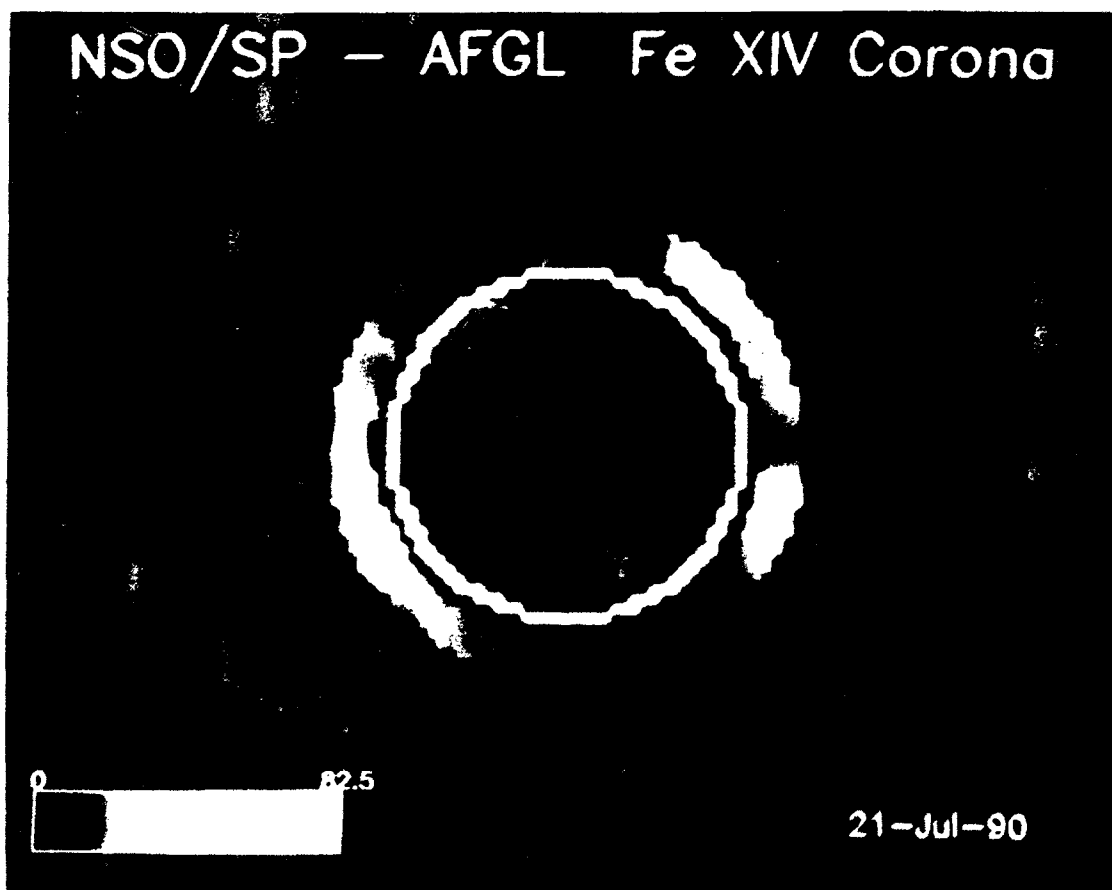

FIGURE 9. Computer display of coronal emissions of Fe XIV near the time of the total eclipse 9 hours before the airbone experiment (16:56 U.T.), as recorded at NSO/SP. Note that the calibration bar gives intensities in millionths of the intensity of the disk at 530.3 nm integrated over a 0.1 nm passband. N is at the top and E at the left.
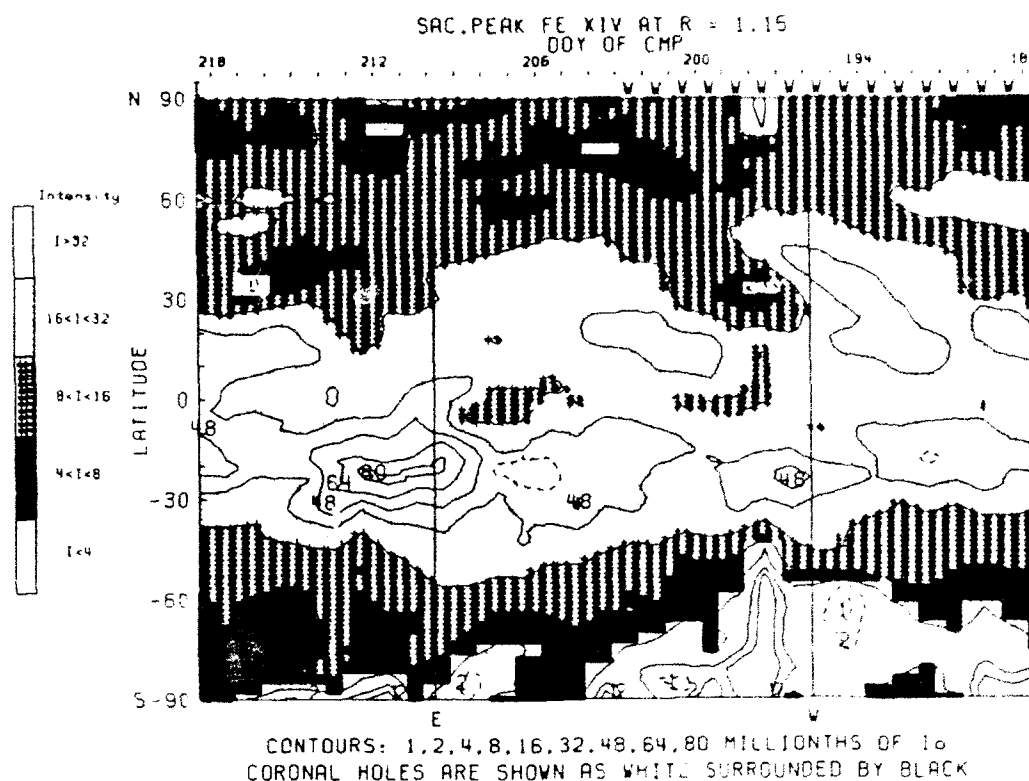
SAC.PEAK FE XIV AT R = 1.15
DOY OF CMP

CONTOURS: 1,2,4,8,16,32,48,64,80 MILLIONTHS OF Io
CORONAL HOLES ARE SHOWN AS WHITE SURROUNDED BY BLACK

FIGURE 10. Synoptic map of Fe XIV emissions at R 1.15 $\pm$ 0.034. This map has been reconstructed using observations made around the eclipse date, using both E-limb and W-limb (denoted by Ws at top) data. Note the CH at the SW. The vertical lines show the position of the limbs at the time of the eclipse.
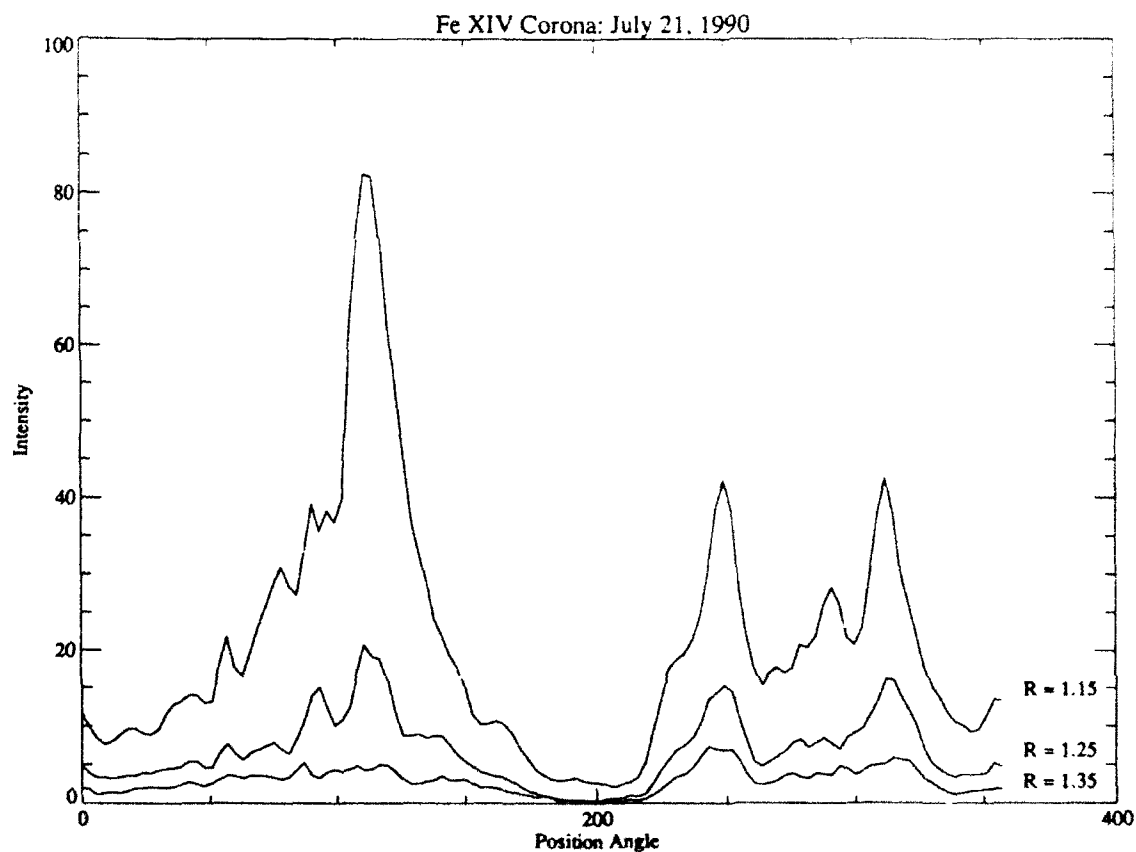
Fe XIV Corona: July 21, 1990

FIGURE 11. Plot of the azimuthal variations of the Fe XIV emission measured 9 hours before the airbone eclipse observations. The total radial extent of the aperture is $0.069 R_\odot$.

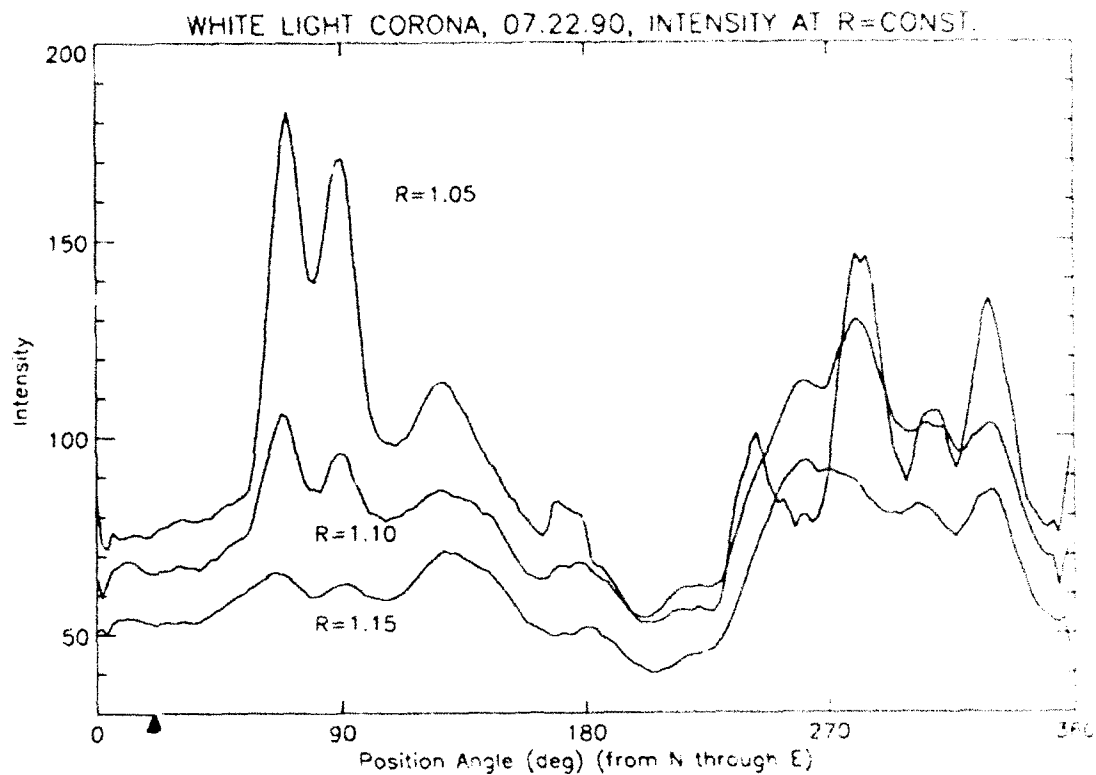## WHITE LIGHT CORONA, 07.22.90, INTENSITY AT R=CONST.

FIGURE 12. Plot of the azimuthal variations of the WL intensities observed in the very inner corona. Note the large intensities due to the emissions by prominences at $R = 1.05$ and 1.10. The exact position of N is near the $20°$ mark.
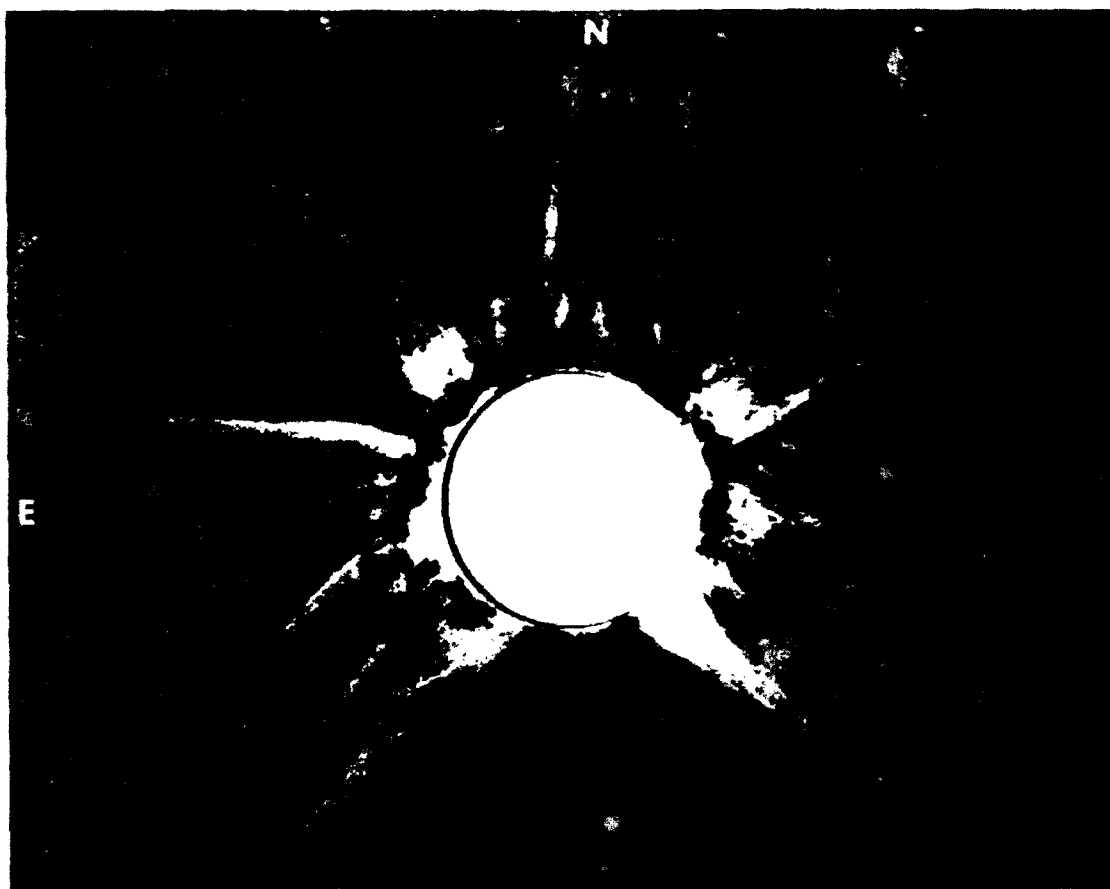

FIGURE 13. Radially filtered ground-based picture of the July 22, 1990 eclipse corona after image processing to increase low-gradient features and to remove artifacts. N is at the top and E is at the left.
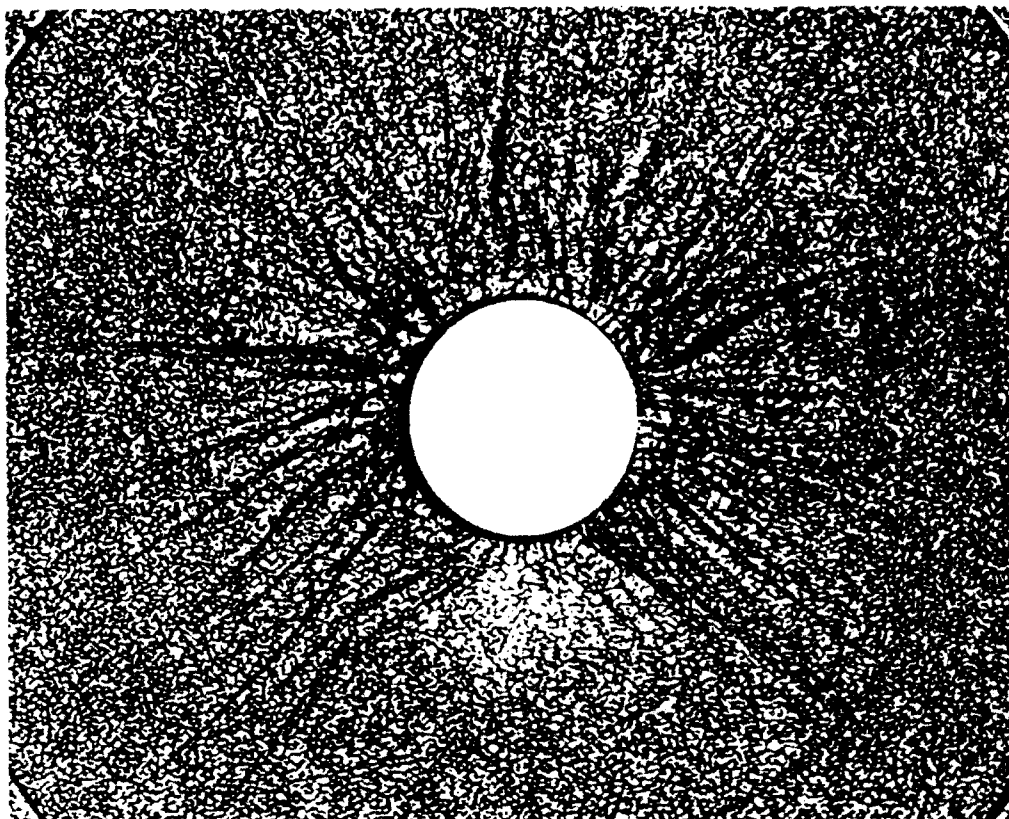
FIGURE 14. As in Fig. 13 to show only small scale gradient features. Note the extended ray at the SW limb, up to $R = 6$
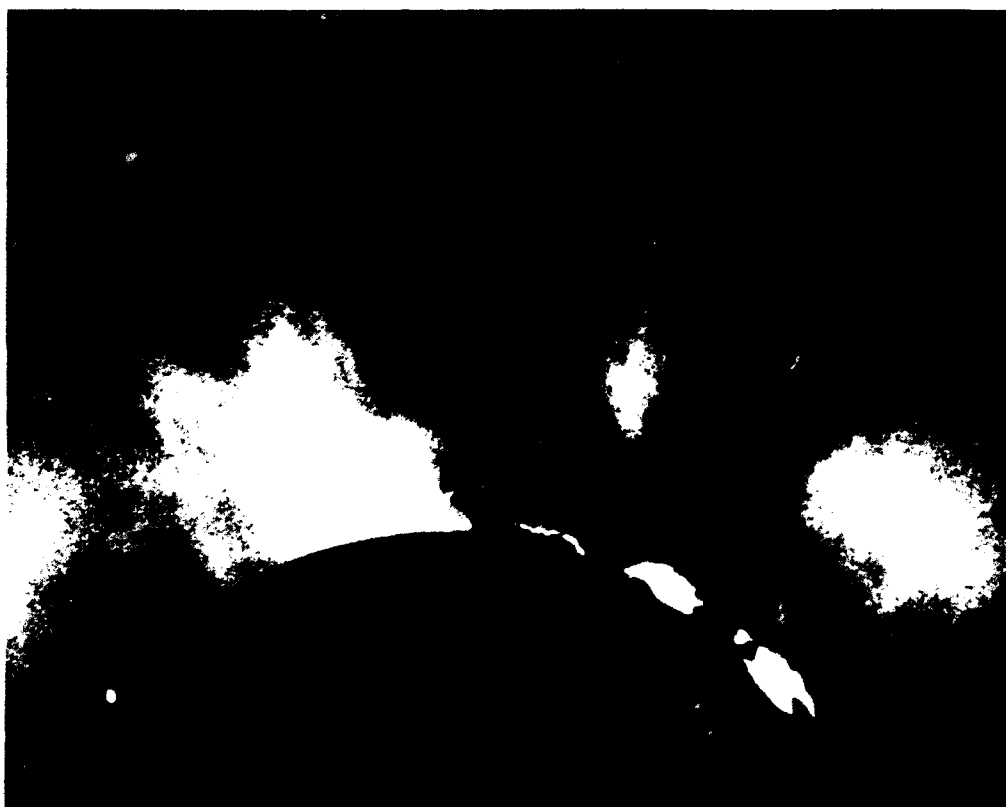

FIGURE 15. Detail of the radially filtered ground-based picture, without any image processing, to show the E limb region. Note the voids rising above the prominences at right and the apparent coronal cavity over the side-on prominence, at left.

REPORT DOCUMENTATION PAGE

4. TITLE AND SUBTITLE	5. FUNDING NUMBERS
Coronal Photometry and Analysis of the Eclipse Corona of July 22, 1990	PE 61102F PR 2311 TA G3 WU 27

6. AUTHOR(S)

S. Koutchmy, R.C. Altrock, T.A. Darvann, N.I. Dzubenko,
T.W. Henry, I. Kim, O. Koutchmy, P. Martinez, C.Nitschelm,
G.A. Rubo, J. Vial ***

7. PERFORMING ORGANIZATION NAME(S) AND ADDRESS(ES)	8. PERFORMING ORGANIZATION REPORT NUMBER
Phillips Lab/GPSS 29 Randolph Road Hanscom AFB, MA 01731-3010	PL-TR-93-2047

9. SPONSORING /MONITORING AGENCY NAME(S) AND ADDRESS(ES)	10. SPONSORING /MONITORING AGENCY REPORT NUMBER

11. SUPPLEMENTARY NOTES   ***AUTHOR AFFILIATIONS ON NEXT PAGE

12a. DISTRIBUTION /AVAILABILITY STATEMENT	12b. DISTRIBUTION CODE
Approved for public release; Distribution unlimited	

13. ABSTRACT (Maximum 200 words)

Abstract. -- An extensive collaborative study of the maximum-type solar corona at the July 22, 1990 eclipse has been performed after collecting data from the ground and from an aircraft. The study provides photometric quality data and structural analysis on the electron corona. Synoptic data are used from the Emission-Line Coronal Photometer of the National Solar Observatory/Sacramento Peak. The activity of the low corona at the time of the eclipse is first discussed. Noticeable is a large nearby polar hole at the SSW limb well-observed on both synoptic green-line data and eclipse data. Strong activity is seen at the E and W limbs and numerous faint prominences are recorded all around the limb. The photometry of the White-Light corona has been performed with selected pictures from the French Falcon-20 aircraft experiment flown above Finland. Isophote maps are given as well as azimuthal scans in absolute units of average solar brightness. The standard flattening index is computed using the values determined for different radial distances. A few scans are compared with Fe XIV 530.3nm scans, and show great similarity when prominence emissions are excluded. The structural analysis is based on the excellent radially-filtered eclipse pictures obtained from the ground with one of the standard multi-station experiments placed along the path of totality in the USSR. Both the inner parts and especially the outer parts of the plasma corona are analyzed. Processed pictures to enhance small-scale gradients show the distribution of streamer-like structures and extremely fine rays. Despite a rather bright sky, long rays are seen up to $6R_\odot$; the origin of several very fine straight coronal threads is discussed, as well as a system of voids seen above the East limb, surrounding prominence material

14. SUBJECT TERMS			15. NUMBER OF PAGES
Sun: Corona - Sun: total eclipse - Sun: atmosphere Sun: activity -prominences - solar wind			14
			16. PRICE CODE

17. SECURITY CLASSIFICATION OF REPORT	18. SECURITY CLASSIFICATION OF THIS PAGE	19. SECURITY CLASSIFICATION OF ABSTRACT	20. LIMITATION OF ABSTRACT
UNCLASSIFIED	UNCLASSIFIED	UNCLASSIFIED	SAR

S. Koutchmy[1,5], R.C. Altrock[2,5], T. A. Darvann[3], N. I. Dzubenko[4], T. W. Henry[5], I. Kim[6], O. Koutchmy[7], P. Martinez[8], C. Nitschelm[1,9], G. A. Rubo[4] and J. Vial[10]

[1] Institut d'Astrophysique de Paris, CNRS, 98 Bis Bd Arago, F75014 Paris, France

[2] Phillips Laboratory (AFSC), Geophysics Directorate, Sunspot, NM 88349, USA

[3] University of Olso, Institute of Theoretical Astrophysics, P. O. Box 1029, Blindern N-0315, Olso 3 Norway

[4] Kiev University, Department of Physics, Kiev-252127, Ukraine, Russia

[5] National Solar Observatory/Sacramento Peak, National Optical Astronomy Observatories*, Sunspot, NM 88349, USA

[6] Sternberg Astronomical Institute, Moscow University, 119899 Moscow, Russia

[7] Univ. Pierre et Marie Curie, Laboratoire Analyse Numérique, Tour 55-65, 4 place Jussieu, 5ème étage, F-75230 Paris Cedex 05, France

[8] Ecole Nationale Supérieure de l'Aéronautique et de l'Espace, B.P. 4032, 31055, Toulouse Cedex, France

[9] Observatoire de Genève, 1290 Sauverny, Switzerland

[10] Institut d'Astrophysique Spatiale, Université Paris XII, Bat. 121, F-91405, Orsay Cedex, France